Chapter 2
Literature Survey and Theory

This part is split into three sub sections. First a brief introduction, covering the studied reactions and their mechanisms is presented. Second, the fundamentals of the electronic structure of model systems and adsorbed species, with a focus on electron emission spectroscopy (EES) are discussed. Last, the motivation for studying catalyst model systems under ambient pressure conditions is introduced, followed by a brief description of thermal stability under applied conditions.

2.1 Chosen Catalytic Reactions

The following sections deals with the reactions studied within this work. For UHV and ambient experiments *CO* oxidation, for UHV *ethene* hydrogenation and for ambient conditions photocatalytic *water* splitting is introduced. As these model reactions are extensively studied in surface science only a brief overview is given. Further, the survey is limited to findings on *Pt* surfaces and *Pt* nanoparticles, in the case of photocatalysis, to semiconductor based systems (i.e. *CdS*).

2.1.1 CO Oxidation

The conversion of *CO* and O_2 into CO_2 in the gas phase has a free enthalpy of –283 kJ/mol and is therefore thermodynamically favored [1, 2]. However, in order to initiate this reaction, the activation energy for the dissociation of O_2 has to be overcome, lowered e.g. by a heterogeneous catalyst. The reaction occurs on *Pt* (and other group VIII metals) surfaces via a **Langmuir-Hinshelwood** (LH) **mechanism** [3–8] with the following steps[1] (Eqs. 2.1–2.4, $*$ represent surface adsorption sites).

[1] Also a low temperature mechanism based on molecular *oxygen* [9, 10] and additional pathways for different surface sites (steps and terraces) [11] are known.

F. F. Schweinberger, *Catalysis with Supported Size-selected Pt Clusters*,
Springer Theses, DOI: 10.1007/978-3-319-01499-9_2,

$$O_2 + 2* \rightleftharpoons 2O* \tag{2.1}$$
$$CO + * \rightleftharpoons CO* \tag{2.2}$$
$$CO* + O* \rightleftharpoons CO_2 * + * \quad (RDS) \tag{2.3}$$
$$CO_2* \rightleftharpoons CO_2 + * \tag{2.4}$$
$$2CO + O_2 \rightleftharpoons 2CO_2 \quad (sum) \tag{2.5}$$

Despite this simple mechanism a few particularities of the reaction need to be mentioned. It is necessary for the *CO* and the O_2 molecule first to be strongly adsorbed (chemisorbed) before reaction takes place [1], a coverage dependent step. Pre-adsorbed *CO* inhibits dissociative *oxygen* chemisorption (a necessary prerequisite for the reaction to happen), whereas a pre-adsorbed *oxygen* layer affects the sticking probability for *CO* only slightly [12]. This phenomenon is commonly known as ***'CO* poisoning'** and needs to be taken into account for experimental considerations. Based on these observations the two key factors influencing the reactivity of a catalyst towards *CO* oxidation are given: First, the chemisorption of *CO* and second, the dissociative adsorption of *oxygen* [13].

Supported ***Pt* clusters**[2] on $MgO(100)$ showed a change in reactivity towards *CO* oxidation atom by atom [15, 16]. Based on TPR and IRRAS results different reaction pathways were assigned [2, 15, 17]. The reactivity as a function of size was also correlated to the corresponding level of the center of the *d*-band [18–21] for each size and thus the efficiency of breaking the *oxygen* double bond [17, 22]. Recent results in a similar size range support the correlation between electronic structure and reactivity [23, 24], additionally stressing the influence of the shape of the catalyst particle. For bigger particles, the different adsorption sites observed for *CO* responsible for the different TPR peaks, were successfully assigned, by comparing it with stepped surfaces [25].

The observed behavior of changing reactivity atom by atom, is particularly intriguing since the *CO* oxidation reaction is one of the classic examples of **structure insensitivity**. This means, its turnover rate is essentially independent of metal dispersion, even though the structure and coordinative unsaturation of exposed metal atoms are known to differ among clusters of different size [7, 26]. However, several examples for insensitivity are known [27] (and herein) for very small sizes and is correlated to the higher binding strength of *CO* on step sites present on these small particles, which contain a higher fraction of *CO* bound to step sites.

Recently the *CO* oxidation reaction on supported *Pt* particles (of different sizes) was studied under **applied conditions** (elevated pressures and temperatures, as well as steady-state conditions) and by means of different techniques. Monitoring changes in plasmon frequency (INPS, Sect. 5.2.2) the reaction as a function of the mole fraction (at ambient pressures) was measured on *Pt* catalysts (2–20 nm size) on SiO_2 and proved to be able to detect *CO* poisoning [28], comparable to UHV results. Similar sized catalysts were investigated under near atmospheric pressures (in a

[2] Previously Pt_x ($x = 1, 2, 3$) on SiO_2 had shown different *CO* adsorption/desorption properties in TPD measurements already [14], however no *CO* oxidation had been studied at that point.

reaction cell) and supported by UHV characterization. TOF and activation energies were extracted and the results were extrapolated to single crystal data, suggesting no size effects in 2–3 nm particles [27, 29]. Catalysts synthesized by colloidal methods and tested in flow reactors, at elevated temperatures, support these findings [7, 30] and the assumption of structure insensitivity. *CO* oxidation on cluster materials produced with atomic size control were recently investigated at elevated pressures and revealed size dependent reactivity which was correlated to a change in particle shape and electronic structure [31]. Lastly, larger nanoparticles (3–9 nm) in μ-reactors showed oscillation behavior for the reaction [32], similar to observations known from Ertl et al. [33].

Measuring the reactivity in these studies, steady-state reaction conditions are present and the change in reactivity as a function of temperature is probed. While running the reaction the temperature is increased, at a certain temperature a sudden increase in turnover is observed and this known as **light off** phenomenon. This behavior is explained by the earlier introduced *CO* poisoning effect. In the low temperature range *CO* has a much higher sticking coefficient than *oxygen* and thus the *CO* molecules occupy all free sites on the catalyst as soon as exposed to the reactant mixture and consequently prevents the catalytic conversion. With increasing temperature the residence time of the *CO* gets shorter and eventually *oxygen* can bind and subsequently react to CO_2—due to stoichiometry each *oxygen* molecule reacts with two *CO* and thus leaves two free surface sites after desorption. In a cascade reaction all available adsorbed *CO* molecules react off and give rise to a sudden increase in CO_2 production. Decreasing the temperature a hysteresis is found, because when cooling the sample, free sites are still available and sustain the conversion down to temperatures below the ignition temperature of the light off [30, 32].

In conclusion, the *CO* oxidation mechanism on *Pt*, and other *d*-metals is well understood and serves as a benchmark reaction to characterize reactivity. However, with respect to behavior for supported metal particles and small clusters under ambient conditions, there is still the need for studies in order to fully understand the role of the size, particularly with respect to the electronic structure.

2.1.2 Ethene Hydrogenation

The decomposition of *ethene* under vacuum has been proven to occur over a family of single crystal surfaces, *Pt*, *Rh*, *Pd*, *Ru* as well as supported *Pt*, *Pd* and *Ni* particles. For *Pt*(111), but also for other *d*-metals, in the absence of *hydrogen*, *ethane* is formed and can be detected when studying thermal desorption of *ethene*, thus the formation of *ethane* occurs via a **self-hydrogenation** [34].

During the thermal decomposition, *hydrogen* is formed on the surface and is able to hydrogenate *ethene* to *ethane*. The rate determining step (RDS) is the $C-H$ bond breaking [35] and the overall reaction is described by the following steps (Eqs. 2.6–2.10).

$$C_2H_4 + * \rightleftharpoons C_2H_4* \tag{2.6}$$
$$C_2H_4* \rightleftharpoons C_2H_3 * + H * \quad (RDS) \tag{2.7}$$
$$2H* \rightleftharpoons H_2 \tag{2.8}$$
$$C_2H_4 * + H* \rightleftharpoons C_2H_5 * + 2* \tag{2.9}$$
$$C_2H_5 * + H* \rightleftharpoons C_2H_6 + 2* \tag{2.10}$$

Based on isotope labeling experiments (TPD, IRRAS) [36–39] it was concluded that the catalytic *ethene* **hydrogenation** reaction on surfaces proceeds as a step wise process of *hydrogen* incorporation. This step wise general mechanism is called the **Horiuti-Polanyi** mechanism [40] and is shown in Eqs. 2.11–2.15 [41].[3]

$$H_2 + 2* \rightleftharpoons 2H* \tag{2.11}$$
$$C_2H_4 + * \rightleftharpoons C_2H_4 * \quad (\pi - bonded) \tag{2.12}$$
$$C_2H_4 * + * \rightleftharpoons *C_2H_4 * \quad (di - \sigma\ bonded) \tag{2.13}$$
$$*C_2H_4 * + H* \rightleftharpoons C_2H_5 * + 2 * \quad (RDS) \tag{2.14}$$
$$C_2H_5 * + H* \rightleftharpoons C_2H_6 + 2* \tag{2.15}$$
$$C_2H_4 + H_2 \rightleftharpoons C_2H_6 \quad (sum) \tag{2.16}$$

As denoted in the equations, *ethene* forms two types of adsorbates on the surface depending on the temperature [44]. Between 37–45 K, **π-bonded** species (associatively chemisorbed) are formed [45, 46], which upon heating above 52 K begins to form a stronger chemisorbed **di-σ** species [47–49] on $Pt(111)$ sitting in a *fcc* 3-fold hollow site [49]. These species are the kinetically relevant ones and the RDS is the recombination of the reactants, which must overcome the strong $di-\sigma$ species [41]. Above ~250 K[4] ***ethylidine*** is formed [49, 50] which is a strongly triple-bond carbonaceous surfaces species that forms a strongly adsorbed and difficult to remove over layer on the *Pt*-surface. Calculations suggest that *ethylidyne* does not directly participate in the reaction mechanism, thus the conversion to *ethane* is likely to proceed via *hydrogen* incorporation [51]. This process increases significantly at higher temperatures [35], but so does the formation of elementary ***carbon*** on the metal surface, at temperatures above 450–500 K. At higher concentrations a graphite layer forms and the organic deposits become immobile, consequently the active sites on the metal are poisoned [34, 35]. At even higher temperatures (~700 K) *ethene* rapidly forms a monolayer of **graphene**. The formation of *carbon* is structure sensitive

[3] The presented mechanism is the simplest proposed hydrogenation mechanism, and also known as competitive Horiuti-Polanyi mechanism, as the reactants *ethene* and *hydrogen* compete for one single class of adsorption sites. In order to explain observations with respect to micro kinetics on heterogeneous catalysts this approach is too simple, however since no kinetic interpretation is done within this thesis, the reader is referred to the literature for a more detailed understanding [42, 43].

[4] At room temperature the hydrogenation reaction of *ethene* is again surface-insensitive because of the size and symmetry of *ethene* [35].

as described above in contrast to the hydrogenation and represents due to catalyst deactivation one of the major problems in industrial processes.

Despite the numerous publications available, two major questions remain (part wise) unanswered [36]. First, the exact mechanism for the formation of *ethylidyne* and its actual role in the catalytic formation of *ethane* and second, a detailed picture of the *ethane* formation including all relevant C_2 moieties.

For the *ethylidyne* species the question arises as to whether it is a simple spectator [52] or does it have a more active role in the hydrogenation of *ethene* [36]. The current opinion is [53], that it does not actively participate in the reaction, however blocks the sites available for *ethene* adsorption [54] or reacts with *hydrogen* and thus indirectly affects the reaction kinetics of hydrogenation [51, 55].

The catalytic hydrogenation probably occurs via the incorporation of *hydrogen* atoms into a weakly adsorbed *ethene*, maybe even on a carbonaceous layer [56]. This *ethene* then forms ethyl moieties and eventually forms *ethane*, released as product form the surface [36, 55, 56]. However, all these processes are competing with the formation of *ethylidyne*. As a consequence of the competitive formation the efficiency of the reaction under vacuum is low and the formation of *ethane* only accounts for a small percentage of the initial amount of *ethene*. For example, measurements found that only 10 % of a saturated *ethene* layer were converted via self-hydrogenation to *ethane* at 283 K [54].

Based on these considerations and experimental evidences a current model for the *ethane* formation on $Pt(111)$ is depicted in Fig. 2.1a, involving both π-bonded and $di-\sigma$ bonded species [49]. The competitive interplay between *ethylidyne* formation and the hydrogenation to form *ethane* [49] is presented as both a reaction scheme and as an energy diagram.

Possible routes to the formation of *ethylidyne* are shown in Fig. 2.1b, despite experimental [34–36, 49, 53, 54, 56–58] and theoretical [44, 51, 59, 60] efforts, the elementary steps involved in the transformation from *ethene* to *ethylidyne* are still debated. Further, the influence of co-adsorbates (i.e. *oxygen*, *CO*) on the reactivity (as a function of coverage) have been studied [39, 53, 57, 61, 62], however are not within scope of this thesis and are not discussed.

Various investigations on *ethene* hydrogenation on **supported (*Pt*) particles** also have been performed [25, 43, 63–66] and the following observations are reported. For the adsorption of *ethene* on *platinum* nanoparticles, the *ethylidyne* species is formed at slightly lower temperatures than 300 K; carbon polymers are already formed at 390–480 K showing no trace of attached *hydrogen* in contrast to single crystals [59]. Hydrogenation studies on *Pt* particles supported on silica (zeolites) indicate a structure insensitive behavior as for $Pt(111)$ [43, 63]. However, for particles supported on SiO_2 and Al_2O_3 with a size below 2 nm a structure sensitivity is observed. For progressively smaller sizes a four times increase in reactivity diminishes below 0.6 nm, until no reactivity was measured [64, 65]. On a more mechanistic level it was mentioned that *ethylidyne* would not be involved in the reaction in the case of supported particles [49, 67] and that in absence of *hydrogen* only the $di-\sigma$ species could be converted to *ethylidyne* [68].

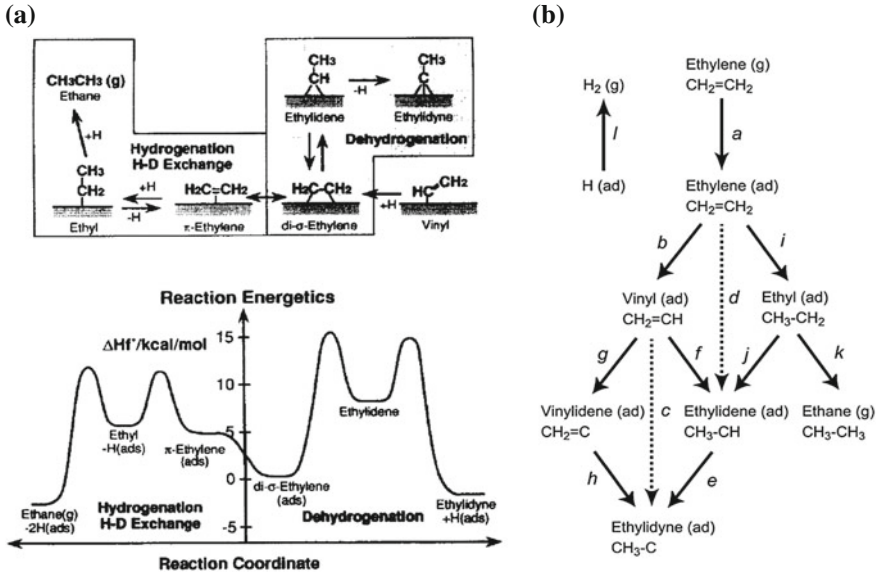

Fig. 2.1 Reaction scheme and energy diagram for the surface chemistry occurring during thermal conversion of *ethene* via hydrogenation on *Pt*(111), (a). The mechanisms shown, for both the conversion of *ethene* to *ethylidyne* (via an *ethylidene* intermediate) and for $H - D$ exchange and hydrogenation reactions (via a common ethyl moiety) [36]. Possible reaction pathways for *ethylidyne* formation over *Pt* group metals at $T > 200\,\mathrm{K}$, (b), three mechanisms are suggested: mechanism 1 (*a*,*b*,*f* and *e*), mechanism 2 (*a*,*b*,*g* and *h*) and mechanism 3 (*a*,*i*,*j* and *e*) [51]. **a** *Reprinted with permission from* [36]-*Copyright (1996) American Chemical Society*. **b** *Reprinted from* [51], *Copyright (2012), with permission from Elsevier*

In summary, the mechanisms of the catalyzed *ethene* hydrogenation reaction (even on simple model surfaces) is far from being settled. A better control on the reaction, i.e. by means of a well defined catalyst might help to shed light on some of these open questions.

2.1.3 Photocatalytic Water Splitting

Photocatalysis is based on the principle, that through adsorption of photons free charge carriers are generated, which supply catalyzed redox reactions with enough energy to get a reaction going. In the case of *water* splitting, the mechanism of photocatalytic *hydrogen* generation as illustrated in Fig. 2.2a, can be divided into three steps: first absorption of photons by a semiconductor material creating electron/hole-pairs, second migration to the surface or recombination, and third surface reduction/oxidation reactions [69].

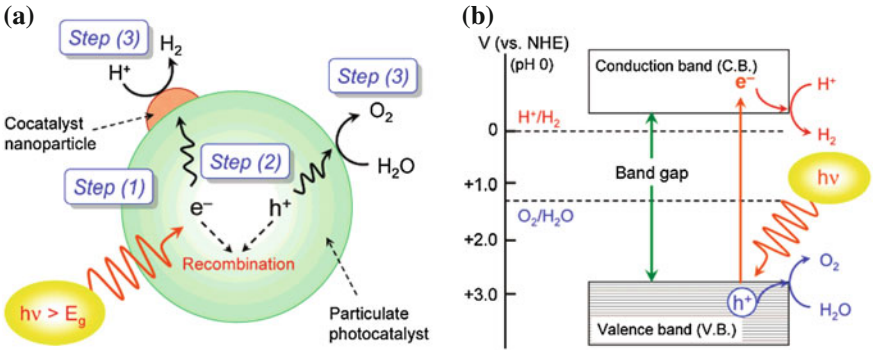

Fig. 2.2 Illustration of the mechanism of photocatalytic *water* splitting and corresponding energy diagram. **a** Process sketch. **b** Energy diagram. The process **a** involves three steps: photon absorption generating electron-hole pairs (step 1), charge-carrier separation (and recombination, step 2) and surface reduction/oxidation reactions (step 3). Schematic energy diagram **b** for exciton mediated *water*-splitting in a semiconductor. A minimum band gap size of 1.23 V versus NHE and suitable band edge positions are prerequisite [70]. *Reprinted with permission from* [70]-*Copyright (2007) American Chemical Society*

A photocatalyst material should adsorb UV-Vis photons efficiently to meet the requirement of using the sunlight as an energy source [69]. This property is determined by the DOS of the underlying semiconductor material. Electronic states in semiconductors, according to the band model, can be described by a valence band (VB) and a conduction band (CB) separated by a band gap (E_g) [71]. Illumination will lead to excitation of electrons from the VB to the CB and generation of empty states (so called 'holes' h^+) at the upper edge of the VB as soon as the photon energy exceeds the band gap ($h\nu > E_g$). Photo generated electrons and holes that subsequently migrate to the surface of the semiconductor without recombination can cause reduction (H_2 formation, $E_{H_2O/H_2} = 0\,V$) and oxidation (O_2 formation, $E_{OH^-/O_2} = 1.23\,V$ or oxidation of a hole scavenger) reactions [69]. The *water* splitting reaction ($2H_2O \rightleftharpoons 2H_2 + O_2$) can be described by the partial equations for reduction (Eq. 2.17) and oxidation (Eq. 2.18) [70].

$$4H_2O + 4e^- \rightleftharpoons 2H_2 + 4OH^- + 4h^+ \quad (red) \tag{2.17}$$

$$4OH^- + 4h^+ \rightleftharpoons O_2 + 2H_2O + 4e^- \quad (ox) \tag{2.18}$$

$$2H_2O \rightleftharpoons 2H_2 + O_2 \quad (sum) \tag{2.19}$$

Since for the formation of the O_2 molecule a complex four hole oxidation is necessary (see Eq. 2.18), the oxidation reaction is quite difficult to achieve. In order to still be able to study the reduction reaction (Eq. 2.17) the oxidation step is replaced by the oxidation of a so called **hole scavenger**. The reduction potential of this scavenger lies energetically above the VB; the oxidation usually requires only one or two holes and can therefore be easily achieved. In the experiments within this thesis, ***TEA***

(triethanolamine) as a sacrificial hole scavenger was used. The disadvantage of a scavenger is, that it gets consumed during reaction (*hydrogen* evolution) and thus the reaction is no longer a cyclic process.[5]

In order for H_2 and O_2 formation to occur at the semiconductor surface the CB edge must be more negative than the reduction potential[6] of the H_2O/H_2 redox couple whereas the upper VB edge must be more positive than the oxidation potential of OH^-/O_2 as illustrated in Fig. 2.2b. These requirements for a semiconductor photocatalyst for *hydrogen* generation give rise to a **minimum band gap of** 1.23 eV, corresponding to a wavelength of 1008 nm. Due to losses from over potentials in various steps of the photocatalytic process, suitable band gaps for real photo catalysts lie in the range of 2 eV ($\leq$ 620 nm) and therefore these systems are in principle capable of utilizing light in the visible range of the solar spectrum [69]. For the discussion of nano structured materials as photo catalysts the above considerations of the general electronic structure of semiconductors are however not quite adequate, since quantum size effects have to be considered. These lead to a distribution of rather individual, discontinuous electronic states and enable the tailoring of the band gap of nanometer size objects by synthetic variation of their composition, shape and dimensions [72, 73].[7]

In the presented case ***CdS***, as a prominent example for nano structured II-VI semiconductors, were used since their lower band gaps compared to corresponding oxide materials make them attractive candidates for visible light assisted photocatalytic *hydrogen* generation. The hole scavenger *TEA* protects the *CdS* from anodic photo corrosion (caused by oxidation reactions, i.e. $CdS + 2h^+ \rightarrow Cd^{2+} + S$) by swiftly consuming the holes, preventing any other oxidation reactions [75]. Using **nanorods (NRs)**, the metal sulfide photo catalysts permit short bulk to surface transfer distances for the charge carriers reducing the probability of electron-hole recombination by control of the rod diameter [69]. NRs are particularly advantageous compared to nano particles, because of their high chemical stability. Their large structures, up to hundreds of nanometers, prevent them better from agglomeration or coalescence [74]. Further, concerning noble metal decoration, it has been shown that these structures can serve as a suitable support for the nucleation and growth of noble metal clusters and larger particles from solution [76, 77].

After photon absorption, charge carrier separation and migration is the next crucial step of photocatalytic *hydrogen* generation. For the formation of *hydrogen* the generated electrons need to be transferred to the semiconductor surface or to a catalytic active metal particle. In a similar way holes must be transferred to the surface, in order to catalyze O_2 formation or the oxidation of a hole scavenger. High photocatalytic

[5] In terms of energy efficiency this makes the performance less productive; thus in perspective of an applied research the reduction potential and the availability of a scavenger needs to be taken into account.

[6] Redox potentials are given with respect to the normal *hydrogen* electrode (NHE) at $pH = 0$.

[7] For example, it was shown that the band gap size of CdS clusters decreases from about 3.6 to about 2.6 eV (bulk CdS $E_g = 2.4$ eV [74]) when increasing the diameter of the clusters from 10 to 60 Å.

activity can only be obtained when competing processes like trapping by surface defects or photoluminescence by electron/hole recombination can be suppressed to some extent [78].

The use of **noble metal particles** as co-catalysts has proven to greatly enhance the photocatalytic activity for *hydrogen* generation [70, 75, 76, 79]. A comparative study on CdS nanoparticles showed that amongst *Pt*, *Pd* and *Rh* the highest *hydrogen* production rate can be obtained over *Pt* metal[8] loaded *CdS* particles [79]. Thus, *Pt* was chosen as the co-catalyst metal. The metal particles act as an efficient sink for photo generated electrons and thereby catalyze the reduction of *water* to *hydrogen* [81].

In order to improve further the efficiency of the *hydrogen* evolution reaction, it is necessary to fully understand the underlying reaction mechanisms. Understanding and controlling the metal co-catalyst is one way to achieve higher reactivity.

2.2 Electronic Structure and EES

This section is dedicated to the main focus of the UHV experiments in this thesis, the electronic structure of metal surfaces, supported metal clusters and adsorbate interactions. In the light of the idea to tune reactivity by the modification of the catalyst (i.e. size) a brief introduction of adsorption and the electronic structure of the catalyst adsorbate interaction is given.[9] Further, an overview over EES results on metal particles and clusters is presented, followed by a sections about EES of adsorbates and the data treatment for comparison to gas phase spectra, applied in this work.

2.2.1 Adsorption

As mentioned, the way of how gases/adsorbates interact with surfaces is of crucial importance and considered as a key step in heterogeneous catalysis [85]. Consequently, in order to understand the nature of heterogeneous catalyst properties, it is essential to investigate the adsorption behaviour of reactants [35, 86]. A comprehensive understanding of adsorption requires detailed information about the electronic properties of the adsorbate-substrate pair [38], as the electronic structure of a surface is an essential factor determining its chemical reactivity [19]. A few thoughts, considerations and models utilized in this work are briefly mentioned in the following.

---

[8] These findings can also be related to *Pt* being the most active metal in electrochemical *hydrogen* evolution, owing to the ideal chemisorption strength of the adsorbed reaction intermediate H^+ corresponding to the Sabatier principle [80].

[9] An introduction to the underlying fundamental solid state theory can be found in the literature [41, 82–84].

The catalytic reactivity of a material can be described by **Sabatier's principle** [41, 87]. It states, that catalytic reactions proceed best if the interaction between reactant/adsorbate and surface is neither too strong, nor too weak[10]; thus the optimum reactivity is related to the heat of adsorption. Sabatier's principle is reflected in **volcano curves** [88], where the reactivity of different elements towards a particular reaction is plotted as a function of its position in the periodic table, and thus its electron(ic) configuration [87]. As a result of experimental and theoretical observations plotted as volcano curves, often *Pt* turns out to be the optimum catalyst material [89]. This is the reason for the choice of *Pt* in this thesis with respect to *CO* oxidation [1, 20] and for the hydrogenation of *ethene* [21, 35], where *Pt* is known to be ideal. The optimum reactivity of *Pt* (compared to other *d*-metals) is further well described using the popular ***d* -band model** [18–21]. The model describes trends in the interaction between an adsorbate[11] and a *d*-metal surface to be governed by the coupling to the metal *d*-bands [90].

Consequently, the bond strength between catalyst and adsorbate, and thus, whether a metal is reactive or not, can be estimated and manipulated changing i.e. the center or the filling, of the *d*-band. In the case of *Pt*, its aforementioned outstanding reactivity (for oxidation and hydrogenation) can be explained by an optimum position of the metal *d*-band. Thus, an ideal ability of the surface to bond to the adsorbates in the sense of Sabatier's principle, based on considerations on the electronic structure [91]. This model also explains, why molecules adsorb more strongly on under-coordinated sites, such as steps and defects, on surfaces. Since the surface atoms on these sites miss neighbors, they have less overlap and will be narrower, leading to a *d*-band shift and consequently a stronger bonding [92]. Based on this insight, the reactivity of supported clusters[12] with under-coordinated sites, can be explained and exploited to fine tune desired chemisorption bond strength and reactivity [15, 22].

Further, the adsorbate surface interaction can be described on the basis of **molecular orbitals (MO)**. Of course, the interaction involves the whole band structure of the solid, however these simplified MO considerations are sufficient to explain and understand the later experimentally observed adsorbate MOs (see appendix Sect. A.3 for gas phase EES spectra [93]) and their changes in the EES spectra. Briefly, the relevant (outermost) MOs for *CO* and *ethene*/*TCE* activation and chemisorption to a surface are summarized.

The **Blyholder model** [94–96] describes the MO interaction of a *CO* molecule at a transition metal surface. The lone pair of electrons on the *carbon* atom (5σ, HOMO) donates into the metal, forming a σ-bond. The *d*-orbitals of the metal donate electron density into the anti-bonding ($2\pi^*$, LUMO) orbital of *CO* giving rise to a π-bond (back donation). The energetic **shift of the** 5σ **orbital** is therefore directly related to the strength of the bond formed between *CO* and the surface (lower 5σ

[10] I.e., in the case of *CO* oxidation the metal should bind neither to strong for the *CO* to poison the surface, nor to weak to not being able to break the *oxygen* bond.

[11] An atom or molecule in front of a metal surface interacts with all valence states of the surface atoms. For a transition metal, a broad s*p*-band and a narrow *d*-band.

[12] Assuming a cluster with enough atoms, to be considered already metallic.

MO, stronger bond). Thus, the lower the energy level of the MO (i.e. high *BE*), the stronger the chemisorption of the *CO* [97].[13] For olefines, a similar MO, the **Dewar Chatt Dunchanson** model is known. As for *CO*, the *ethene* molecule donates π-electrons of its lone pair (HOMO) into a *d*-metal with the right symmetry and forms a σ-bond. By means of a back donation the *d*-orbitals of the metal donate electron density back into the $\pi*$ orbital (LUMO) of the olefin, weakening the $C = C$ bond, while the metal olefin π-bond gets stronger [98, 99]. The stronger the bond of the molecule to the surface, the lower the energy of the *ethene* HOMO, thus as measure of chemisorption strength the **BE of the *ethene* π_{C-C} is decisive**.

In cases of **substitute groups** on the olefine (i.e. chlorine), the different substitutes of the alkene alter its electronic structure and therefore the energy levels of the MOs. Dependent on the electronegativity of the substitute groups the strength of the $C = C$ bond is influenced [93, 100]. Using **substitute groups** such as halogens, the **strength of the *C=C* bond is lowered**. Consequently, in the case of i.e. *TCE*, the interaction with the metal for both donation and back-donation gets less and chemisorption is more difficult. Further, the additional substitute groups attached to the olefine render the molecule more **stericly demanding**, complicating a strong chemisorption bond to the metal [101].

2.2.2 EES of Supported Clusters

From an experimental perspective, electron emission spectroscopy is probably the most important and often used technique to investigate the (valence) electronic structure [102]. The following briefly discusses the major results of the last few decades gained by means of EES with respect to clusters (without adsorbates). In contrast to gas phase PES [103, 104], conventional EES of supported clusters yielded little information [22].

For the first EES of supported 'clusters' reported, deposition was performed by **metal evaporation** and thus the experiments suffered form poor cluster size control and increase in size with the deposited amount [102, 105]. However, the evolution of deposited atoms/clusters to bulk properties were observed for *Ag* on SiO_2 [106], *Pt* and *Pd* on *C* [107] by means of XPS. In the case of silver, bulk features were established at a coverage of 5×10^{15} atoms/cm^2 and were preceded by a shift towards lower binding energy (BE) for increasing coverages in the low BE energy threshold of the EES spectrum by approximately 2.5 eV and the appearance of the spin-orbit split Ag 4*d* peaks. A similar behavior, was observed for *Pt* and *Pd* as a function of coverage. The most prominent feature of the EES however, was the onset

[13] The 5σ and 1π orbital are almost energetically degenerate, as a consequence of chemisorption and thus, the extent to which these MOs are joined is another marker of the strength of chemisorption.

of electron density at E_f and a bulk *Pd* behavior at 14×10^{15} atoms/cm^2 [108].[14] The origins of the aforementioned core level shifts were discussed in relation to final and initial state effects and as a function of 'size', based on growth models for the chosen deposition method [105, 109].

Later experiments, promoted through the development of **sophisticated cluster sources**, first 'real' EES data of size-selected *Pt* clusters was obtained and clarified earlier observations [110–112]. Comparing IP of *Pt* atoms and dimers, the support was seen to induce a 1.6–1.8 eV negative shift in IP due to final state screening (explanation see Sect. 2.2.3), suggesting that clusters of this size were not metallic. Also, the valence electronic structure was probed as a function of cluster size, showing the characteristic *Pt* spin-orbit split photoemission peaks. However, the experiments were performed using cluster coverages at which aggregation of the clusters cannot be ruled out and thus contradict observations made for similar systems in gas phase [96]. More recently experiments, present no new insights except, that EES (UPS) of 'size-selected' Ag_{923} and Ag_{25} clusters is achievable while assuring that no agglomeration[15] occurs [113]. Selected *Pt* clusters supported on TiO_2 probed by means of XPS [31], showed size-dependent shifts towards lower BE for increasing size, in agreement with the above literature.

Concerning MIES, only in the last decade and considerably few attempts have been done towards elucidating the electronic structure of supported catalyst materials. On *MgO* the alkali metals *Na* and *Li* have been probed [114] as well as *Ag* [115], deposited via vapor deposition—in either case the metals could hardly be detected and only at high coverages. Further, *Pd* on *MgO* was probed revealing small features at extreme high coverages [116, 117], the authors consider that a reduction in particles size beyond 1 nm will give rise to the change of the interaction process between He* and the adsorbate from AN to AD as soon as the transition from metallic-like to molecular behavior of the cluster takes place.

2.2.3 Photoemission of Adsorbates: Data Treatment

Photoemission experiments have been shown to provide much insight into the electronic structure of the adsorbate/adsorbent interaction [64, 97, 118]. Thus, this section is dealing with the peculiarities and problems of these techniques for the study of adsorbate interaction and approaches used in this thesis. General choices for data treatment are presented and explained, the interpretation is subject of the following section. The considerations are based on the general knowledge on PES/EES, the (experimental) principles are briefly introduced in the Chap. 3 in Sect. 3.2.5.

[14] Within this work also *CO* was dosed on the surface and the resulting UP spectrum revealed the expected *CO* MO peaks, which were shifted about +0.5 eV compared to of single crystal data thus indicating a possible cluster induced effect [108].

[15] Using lower coverages additionally characterized by means of STM.

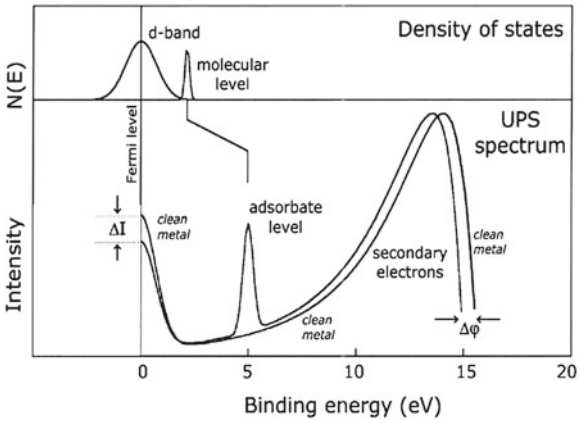

Fig. 2.3 Schematic UPS spectra of adsorbed species on a *d*-metal and the corresponding DOS of the metal and MOs of the adsorbed species [119]. *J.W. Niemantsverdriet: Spectroscopy in Catalysis: An Introduction, page 69. 2007. Copyright Wiley-VCH Verlag GmbH & Co. KGaA. Reproduced with permission*

The general picture of a EES experiment of an adsorbate on a *d*-metal, including the changes to the spectrum, can be seen in Fig. 2.3. The important features are the change $\Delta\phi$ in the work function (WF), attenuation of the *d*-band signal, ΔI, and the presence of adsorbate photoemission peaks. The change in WF can be explained using the jellium model as a simple description. An adsorbed species changes the dipole layer of the surface (depending on the dipole moment of the adsorbate) which is the surface contribution to the WF and this changes its value. The attenuated *d*-band intensity is changed because the adsorbed gas reduces the photo emission of the substrate [119].[16]

With the intention to study the adsorbate-substrate/catalyst interactions the occurrence of adsorbate peaks originating from the corresponding MOs are of paramount interest. In particular, a comparison with gas phase PE spectra of the free molecule can yield information on the MO interaction with a surface, which manifests itself as a shift in the IP of the adsorbate's MO [97, 99, 120, 121]. Further, the changes in the WF of the adsorbent can reveal more information on the nature of the interaction as well as corroborate conclusions reached by studying the shift of IPs.

In gas-phase studies the electron BEs are commonly **referenced to the vacuum level** and plotted on an ionization potential (IP) scale, whereas in the study of solids, E_F provides the experimental reference point on a BE scale (with $E_F = 0$) [101]. Thus, in order to compare gas phase spectra with spectra of adsorbed molecules

[16] However, this does not need to be interpreted as an electron flow from the *d*-band into the unoccupied states of the adsorbate.

on a surface, the BE scale of the latter is converted into IP energy scale.[17] For this purpose the WF has to be added to the measured electron BE. It is usual practice to reference with respect to a fixed WF value, either the WF of the clean substrate as recommended by Broughton et al. [122] or by using the WF of the saturated surface as suggested by Kelemen et al. [97, 101]. The practice of using a fixed WF reference point accounts for the fact that usually adsorbate BE (measured with respect to E_F), which belong to non-interacting orbitals, are fixed in energy when increasing the adsorbate coverage; although the WF is coverage dependent [101, 122]. Further details on the argumentation on the so called 'reference level problem' can be found in the literature [123, 124]. For referencing the EE spectra of this work, the WF of the clean metal substrate as indicated in Eq. 2.20 is added, thus following the procedure suggested by Broughton et al.:

$$IP_{solid} = BE_{solid} + \phi_{clean\,surface} \tag{2.20}$$

Furthermore, as seen in the sketch in Fig. 2.3, at high IP energies an increasing amount of **secondary electrons** [86, 119] are present. These electrons have undergone inelastic collisions and additional scattering events while traveling through the specimen and therefore contain no meaningful information about the electronic structure [97, 121]. Unfortunately, these electrons also suppress features from the adsorbed molecule in the spectra. In order to reveal features obscured by these secondaries, it is a common approach to subtract a fit function [125]; for the spectra in this work a polynomial function is fitted to the spectra and subtracted from the original spectrum [126].

A more detailed description of this approach, along with the used peak fitting procedure and details on the parameters, is stated in the appendix in Sect. A.1.5.

2.2.4 Interpretation of BE Shifts of Adsorbates in EES

Comparing gas phase spectra of the free molecules with that of adsorbed ones, two observations are made: loss of rotational fine structure, thus broadening of peaks, and a **shift in energies** on an IP scale. The extent of the energy shift reflects the state of the adsorbed molecule [101, 118]. However these shifts ΔE_B compared to the gas phase values cannot be directly related to chemical properties since they consist of mainly two parts that can be separated in contributions from physical adsorption, called **'relaxation shifts'** ΔE_{RV} and chemical adsorption ΔE_{BOND} (Eq. 2.21) [97, 118].

[17] It is noteworth, that this conversion of BE to IP still fails to completely define the adsorbate surface interaction in terms of the molecular orbitals of the adsorbate. In the case of UPS this is largely due to the fact that it is an integral technique and therefore probes a very large number of molecules at once, while at the same time requiring relatively high coverages (1 *ML*) to resolve individual peaks [97]. Only with a local technique at very low coverage, i.e. in the absence of adsorbate-adsorbate interactions which can lead to a 1 eV shift, can the true adsorbate electronic structure be realized.

$$\triangle E_B = \triangle E_{RV} + \triangle E_{BOND} \tag{2.21}$$

For **physisorption**, the valence band peaks belonging to MOs are found to shift towards lower IP compared to the gas phase values. Most of this effect can be accounted for as a **final state** effect, where the electron hole from the emitted electron is screened by surrounding molecules and the surface [97], thereby increasing the KE of the emitted electrons and lowering the IP [99]. This energy shift (ΔE_{RV}) is referred to as '**relaxation energy**' [118, 127] although it also contains a potential energy contribution which depends on the adsorption geometry in front of the surface [123].

For core-level BE the observed relaxation shifts (ΔE_{RC}) are usually bigger, as the presence of valence-electron reservoir in the metal allows the molecular equivalent of outer-shell relaxation, as electron charge is transferred into the molecule's valence orbitals during photoemission. Concerning the size of the molecule, the larger the molecule, the less the observed relaxation shift as the created hole charge tends to be screened already in the molecule itself [118].

In the case of **chemisorption**, the shifts oppose the trend observed and shift to higher BE/IP. The cause is an **initial state** effect, due to the change in the chemistry of the molecule [99], where the **bonding MO is lowered**[18] in energy [128].

The different changes expected in EES along with their energy shifts upon adsorption of a molecule are summarized in Fig. 2.4. The energy level diagram highlights again, that due to the possible convolution of the introduced initial and final state effects, it is difficult, to gain clear chemical information from EES if both physisorption and chemisorption occur [124].

Last, with respect to the differences found in the application of UPS and MIES for probing adsorbates, **symmetry considerations** are necessary. For UPS an additional selection rule based on symmetry needs to be applied, that has a polarization dependency of the light [96, 97]. Thus, the orientation of the adsorbate orbitals and the polarization of the incoming light both play a decisive role in the photoemission of an electron in UPS. Applying Fermi's Golden Rule, the photoemission experiment only detects electrons that lead to a total symmetric dipole transition matrix element and the final state of the photoemission is necessarily gerade. If the incident light is *s*-polarized then it has ungerade symmetry in the emission plane and in order for the transition matrix element to be non-zero, the initial state must also be ungerade. This occurs for *p*-orbitals that are parallel to the surface plane (i.e. 1π or $2\pi^*$ in the case of *CO*, as it is known to adsorb perpendicular to the surface in many cases). If the incident light is *p*-polarized then it has gerade symmetry and therefore only gerade initial states will photo emit (for *CO*, 5σ and 4σ).

For MIES, other selection rules apply which are not considered in this thesis. The UPS setup in this work uses unpolarized light, thus contributions of both *s*-and *p*-polarized light can be seen.

[18] For the particular case of C_2H_4 chemisorption the important MO to observe is the π_{C-C} MO, a high BE/IP corresponding to a strong bond [99].

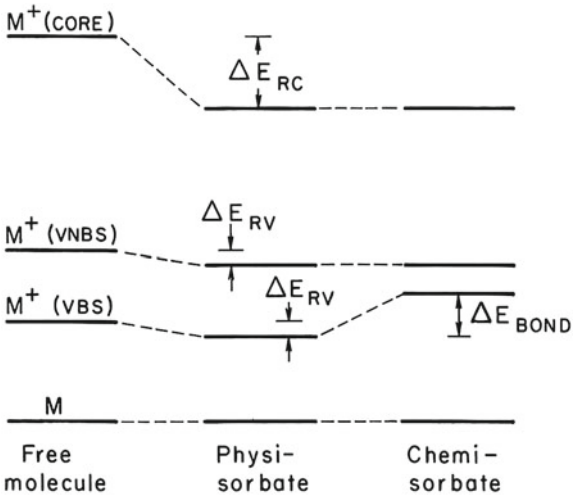

Fig. 2.4 Energy level diagram for EES (on an IP scale) from an adsorbate molecule, showing ground state M, core-hole state $M^+(core)$, as well as hole states $M^+(VBS)$ and $M^+(VNBS)$ of binding and non-binding valence orbitals to the substrate, respectively. Hole-state energies (BE) are lowered (ΔE_{RV}) upon physisorption, because of screening by the substrates (note the bigger relaxation for core holes ΔE_{RC}). Upon chemisorption, the bonding orbital can be identified by an increase ΔE_{BOND} in BE, may however include contributions of ΔE_{RV} [118]

2.3 Model Catalysts Under Ambient and Applied Conditions

In this section the motivation and common approaches for the study of model catalyst materials under ambient conditions is further elucidated. Additionally, in the context of the performed experiments, a short introduction into the stability of supported catalysts is given.

2.3.1 Materials and Pressure Gap

The understanding of surface reactions in general, with respect to catalytic reactions, was predominantly achieved using surface science [64, 86, 129]. Most of these findings, however were obtained on idealized systems and under idealized conditions, mainly on single crystals at low pressure and temperature conditions. The **dilemma of the traditional surface science approach** becomes apparent. Investigations of real catalysts (complex materials), conducted under relevant conditions by *in − situ* techniques, provide little information on the surface of the catalyst, because the techniques which are surface-sensitive can often only be applied on model surfaces under particular conditions (e.g. vacuum). Further, despite being able to describe a catalytic reaction on a well-defined single crystal of a metal under well defined

and simplified conditions, this becomes tremendously more complicated when the same reaction runs over small catalyst particles on a support in a realistic reactor environment [119].

In this perspective, gaps between catalysis and traditional surface science have been identified in the mid 1980s: the '*pressure gap*' [130], the '*materials gap*' [131] and sometimes the '*complexity gap*'[19] [132]. Bridging these gaps are still important [119] and current issues in catalysis [133].

The first approaches to overcome these gaps were so-called single crystal approaches. The bridge to more realistic conditions was established by simply **extrapolating the results** from UHV/single crystal experiments to industrial conditions [134].[20] Considering the difference of roughly ten orders of magnitude in pressure and simplification of the reaction [131] this is a rather surprising result and does not work, but for a few examples [134, 137].

In order to overcome the **materials gap**, more complex surfaces under UHV conditions are studied. In particular, moving from single crystal surfaces towards metal oxide supported particles with different sizes and complexity. These model catalyst surfaces have significantly contributed to a better understanding [35, 64, 138–143]. Beside these supported particles, prepared in UHV usually by means of deposition by evaporation processes [27], other means of preparing model catalyst surfaces are know, e.g. using lithography [129, 144–146]. Except, for a few examples (as the use of size-selected supported clusters in this work) the prepared model materials often lack **reproducibility**, thus the majority of experiments cannot be reproduced and compared [26]. Furthermore, all these more realistic, model systems also mark only another way point, since the structure and chemical composition of a catalyst in operation will be largely determined by dynamic processes. This is problematic, since static conditions, typically applied in surface science, become increasingly irrelevant with increasing rate and pressure [134].

Therefore, by using these more sophisticated materials, two major strategies towards bridging the **pressure gap** have been pursued. On one hand there is the popular approach of **adapting conventional surface science techniques** to work at **elevated/high pressures for *in-situ* measurements** [24, 27]. This has been successfully achieved for a wide variety of instruments, i.e. STM [53, 147, 148], XPS [137] or (E)TEM [149–151]. Other, (optical) techniques have been readily applied at higher pressures as well, e.g. IRRAS [29, 152], S-SHG [49] or FEM [153]. On the other hand, a current trend in achieving insight at elevated pressures and more realistic conditions is the application of **new characterization methods**, such as micro-reactors [154, 155] or sensing devices, exploiting different physical properties [156–159].

Despite the mentioned efforts being only a rough and only partial overview on the current work on the materials and pressure gap, it is still a way to go until conventional

[19] The complexity gap is covering the study of gas and mass transport phenomena, which additionally to materials and pressure gaps need to be considered [132].

[20] The first example was the calculation of the rate of *ammonia* formation under industrial conditions [130, 131], based on well studied single-crystal surface reactions [1, 135, 136].

surface science allows for ultimate insight into the 'work' of an industrial catalyst. Using sophisticated model catalyst systems and a variety of different techniques, this work helps to contribute bridging the gaps.

2.3.2 Stability

With respect to reactivity studies of model catalysts, but also during application in industrial processes of 'real' catalysts, the stability and possible deactivation of a catalyst is a problem of great concern for both [160, 161]. In either case, good knowledge of the stability of the catalyst is a prerequisite for the study of its reactivity, however, often catalyst reactivity is probed [25, 27, 29], with addressing little attention to its stability.

Causes of deactivation are basically three-fold: chemical, mechanical or thermal—hereby six different routes of deactivation of catalyst material are described (some have been introduced before, without further explanation): poisoning (i.e. *CO* on *Pt*), fouling (i.e. coke formation during *ethene* hydrogenation on *Pt*), thermal degradation, vapor compound formation accompanied by transport, vapor-solid and/or solid-solid reactions, and attrition/crushing [162, 163].

Within focus on the ambient part of this work the **thermal deactivation**, and more particular sintering as temperature induced degradation mechanism is studied. Three mechanisms for crystallite growth are known and advanced: crystallite migration, atomic migration and vapor transport. These processes can in general be accelerated by promoters (i.e. *water* vapor, *oxygen*) and are usually irreversible.

Since vapor transport requires very high temperatures it is unlikely to happened in the conducted experiments, the two remaining possible mechanisms of particle growth are: Ostwald ripening (interparticle transport) or particle coalescence and are briefly introduced on an qualitative basis, further information in the literature [149, 164]. Figure 2.5 shows illustrations for the two processes along with theoretical particle size distributions (PSD)—as an initial PSD, the ideal case of a Gaussian distribution is taken (of course this varies with synthesis process). In general, the sintering of small metal particles on an oxide support are driven by a favorable, lower total energy of the particle, due to the loss of surface area and further enhanced by the additional lower surface free energy when uncovering the support surface [41].

The minimization of the surface free energy is the driving force for particle **coalescence** (merging of particles) after **migration** of particles over the surface. The movement of the surface atoms at elevated temperatures induces a Brownian type movement of particles on the surface and eventually two meeting particles coalescent and become one particle. The total number of particles decreases as larger particles are formed on the expense of smaller ones. With respect to the PSD the number of larger particles will rise, while the distribution in general will decrease in size—a particular characteristic is the tail towards larger particles. During **Ostwald ripening** the larger particles grow at the expense of smaller ones, as atoms get detached from

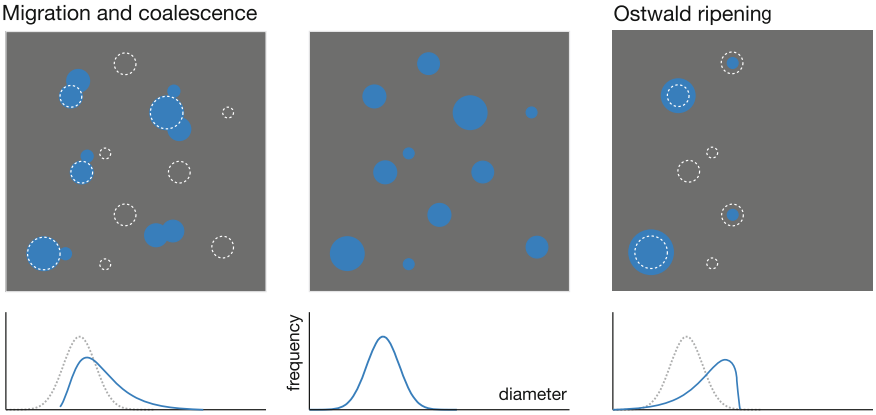

Fig. 2.5 Schematic illustration of Ostwald ripening (*right*) and Migration and coalescence (*left*) sintering processes of particles on surfaces. Below are shown the corresponding, theoretically to expect PSD

the smaller ones and subsequently attached to the bigger particles. When the sintering process is advanced, a decrease in the number of particles is expected, as atoms move to the larger particles and smaller ones 'disappear'. The maximum of the PSD is shifted to higher values with a sharp cut-off; however, the tail of the distribution faces towards smaller particles as a consequence of the continuous supply of smaller particles [149, 165].

The different mechanisms can in general be distinguished by their 'tail' of the PSD, even if this argumentation might be considered part-wise invalid based on experimental observations [166]. Concerning the temperature, when to expect sintering, the correlation with characteristic physical properties is useful [161]. The so-called Tamman and Hüttig temperatures, are directly related to the melting temperature. In the case of *Pt*, sintering is expected from $T_{Hüttig} = 0.3T_{melting} \approx 608\,\mathrm{K}$, for small particles, already at lower temperatures. These observations also justify the use of metal oxides as support materials, as they are considered thermostable. In order to study sintering phenomena on a local level, particularly TEM [167, 168] and STM [169], have shown to be precise methods with insights into the fundamental mechanisms are, however disregard ensemble effects. Therefore, methods close to application [163, 164, 170] are the usual choice; new methods, correlating local phenomena with integral methods are highly desirable.

References

1. Ertl, G. (1994). *Surface Science*, *299–300*, 742.
2. Heiz, U., Sanchez, A., Abbet, S., & Schneider, W.-D. (1999). *The European Physical Journal D: Atomic Molecular, Optical and Plasma Physics*, *9*, 35.

3. Campbell, C. T., Ertl, G., Kuipers, H., & Segner, J. (1980). *Journal of Chemical Physics*, *73*, 5862.
4. Ertl, G., Neumann, M., & Streit, K. (1977). *Surface Science*, *64*, 393.
5. Engel, T., & Ertl, G. (1979). In D. D., Eley, H. P., & P. B., Weez (Eds.), *Advances in catalysis* (Vol. 28, p. 1). San Diego: Academic Press.
6. Ertl, G. (1980). *Pure and Applied Chemistry*, *52*, 2051.
7. Allian, A. D., Takanabe, K., Fujdala, K. L., Hao, X., Truex, T. J., & Cai, J., et al. (2011). *Journal of the American Chemical Society*, *133*, 4498.
8. Engel, T., & Ertl, G. (1978). *Journal of Chemical Physics*, *69*, 1267.
9. Matsushima, T. (1983). *Surface Science*, *127*, 403.
10. Zambelli, T., Barth, J. V., Wintterlin, J., & Ertl, G. (1997). *Nature*, *390*, 495.
11. Xu, J., & Yates, J. T. (1993). *Journal of Chemical Physics*, *99*, 725.
12. Ertl, G. (2001). *Chemical Record*, *1*, 33.
13. Kunz, S., Schweinberger, F. F., Habibpour, V., Röttgen, M., Harding, C., & Arenz, M., et al. (2010). *Journal of Physical Chemistry C*, *114*, 1651.
14. Heiz, U., Sherwood, R., Cox, D., Kaldor, A., & Yates, J. J. (1995). *Journal of Chemical Physics*, *99*, 8730.
15. Heiz, U., Sanchez, A., Abbet, S., & Schneider, W.-D. (1999). *Journal of the American Chemical Society*, *121*, 3214.
16. Sanchez, A. (2000). Ph.D. thesis, Unversité de Lausanne.
17. Heiz, U., Sanchez, A., Abbet, S., & Schneider, W. D. (2000). *Chemical Physics*, *262*, 189.
18. Hammer, B., & Norskov, J. K. (1995). *Nature*, *376*, 238.
19. Hammer, B., & Nørskov, J. K. (1995). *Surface Science*, *343*, 211.
20. Ruban, A., Hammer, B., Stoltze, P., Skriver, H., & Nørskov, J. (1997). *Journal of Molecular Catalysis A: Chemical*, *115*, 421.
21. Hammer, B., & Nørskov, J. (2000). *Advances in catalysis*, *45*, 71.
22. Meiwes-Broer, K.-H. (2000). *Metal clusters at surfaces: Structure, quantum properties, physical chemistry* (1st ed.). Berlin: Springer.
23. Kaden, W., Wu, T., Kunkel, W., & Anderson, S. (2009). *Science*, *326*, 826.
24. Watanabe, Y., & Isomura, N. (2009). *Journal of Vacuum Science & Technology A*, *27*, 1153.
25. Lundwall, M. J., McClure, S. M., & Goodman, D. W. (2010). *Journal of Physical Chemistry C*, *114*, 7904.
26. Boudart, M. (2000). *Topics in Catalysis*, *13*, 147.
27. McClure, S. M., Lundwall, M., Zhou, Z., Yang, F., & Goodman, D. W. (2009). *Catalysis Letters*, *133*, 298.
28. Larsson, E. M., Langhammer, C., Zorić, I., & Kasemo, B. (1091). *Science*, *2009*, 326.
29. McClure, S. M., & Goodman, D. W. (2011). *Topics in Catalysis*, *54*, 349.
30. Santos, V. P., Carabineiro, S. A., Tavares, P. B., Pereira, M. F., Órfão, J. J., & Figueiredo, J. L. (2010). *Applied Catalysis B: Environmental*, *99*, 198.
31. Watanabe, Y., Wu, X., Hirata, H., & Isomura, N. (2011). *Catalysis Science & Technology*, *1*, 1490.
32. Jensen, R. (2012). Ph.D. thesis, Danmarks Tekniske Universitet.
33. Ertl, G. (2007). In Noble lectures chemistry; Noble Foundation.
34. Godbey, D., Zaera, F., Yeates, R., & Somorjai, G. A. (1986). *Surface Science*, *167*, 150.
35. Somorjai, G. (1994). *Introduction to surface chemistry and catalysis* (Vol. 2). New York: Wiley-Interscience.
36. Zaera, F. (1996). *Langmuir*, *12*, 88.
37. Zaera, F., & Somorjai, G. A. (1984). *Journal of the American Chemical Society*, *106*, 2288.
38. King, D. A. (1984). The chemical physics of solid surfaces and heterogeneous catalysis: Chemisorption systems, Part B: 3. In D. A. King, & D. Woodruff (Eds.), *The chemical physics of solid surfaces and heterogeneous catalysis* (Vol. 3). Toronto: Elsevier Science Ltd.
39. Salmeron, M., & Somorjai, G. A. (1982). *Journal of Physical Chemistry*, *86*, 341.
40. Horiuti, I., & Polanyi, M. (1934). *Transactions of the Faraday Society*, *30*, 1164.

41. Chorkendorff, I., & Niemantsverdriet, J. W. (2007). *Concepts of modern catalysis and kinetics* (2nd ed.). Boca Raton: Wiley-VCH.
42. Dumesic, J. A., Rudd, D. F., Aparicio, L. M., Rekoske, J. E., & Treviño, A. A. (1993). *The microkinetics of heterogeneous catalysis* (1st ed.). ACS professional reference book. American Chemical Society.
43. Rioux, R. M., Komor, R., Song, H., Hoefelmeyer, J. D., Grass, M., & Niesz, K., et al. (2008). *Journal of Catalysis*, *254*, 1.
44. Zhao, Z., Moskaleva, L. V., Aleksandrov, H. A., Basaran, D., & Rösch, N. (2010). *Journal of Physical Chemistry C*, *114*, 12190.
45. Cassuto, A., Kiss, J., & White, J. (1991). *Surface Science*, *255*, 289.
46. Cassuto, A., Mane, M., Jupille, J., Tourillon, G., & Parent, P. (1992). *Journal of Physical Chemistry*, *96*, 5987.
47. Hatzikos, G., & Masel, R. (1987). *Surface Science*, *185*, 479.
48. Watson, G. W., Wells, R. P. K., Willock, D. J., & Hutchings, G. J. (2000). *Journal of Physical Chemistry B*, *104*, 6439.
49. Cremer, P. S., Su, X., Shen, Y. R., & Somorjai, G. A. (1996). *Journal of the American Chemical Society*, *118*, 2942.
50. Kubota, J., Ohtani, T., Kondo, J. N., Hirose, C., & Domen, K. (1997). *Applied Surface Science*, *121*, 548.
51. Aleksandrov, H. A., Moskaleva, L. V., Zhao, Z.-J., Basaran, D., Chen, Z.-X., Mei, D., et al. (2012). *Journal of Catalysis*, *285*, 187.
52. Beebe, T. P., & Yates, J. T. (1986). *Journal of the American Chemical Society*, *108*, 663.
53. Tang, D. C., Hwang, K. S., Salmeron, M., & Somorjai, G. A. (2004). *Journal of Physical Chemistry B*, *108*, 13300.
54. Öfner, H., & Zaera, F. (1997). *Journal of Physical Chemistry B*, *101*, 396.
55. Zaera, F., Janssens, T. V., & Öfner, H. (1996). *Surface Science*, *368*, 371.
56. Öfner, H., & Zaera, F. (2002). *Journal of the American Chemical Society*, *124*, 10982.
57. Grunes, J., Zhu, J., Yang, M., & Somorjai, G. A. (2003). *Catalysis Letters*, *86*, 157.
58. Fischer, T., & Kelemen, S. (1977). *Surface Science*, *69*, 485.
59. Watwe, R. M., Cortright, R. D., Nørskov, J. K., & Dumesic, J. A. (2000). *Journal of Physical Chemistry B*, *104*, 2299.
60. Chen, Y., & Vlachos, D. G. (2010). *Journal of Physical Chemistry C*, *114*, 4973.
61. Berlowitz, P., Megiris, C., Butt, J. B., & Kung, H. H. (1985). *Langmuir*, *1*, 206.
62. Cassuto, A., Touffaire, M., Hugenschmidt, M., Dolle, P., & Jupille, J. (1990). *Vacuum*, *41*, 161.
63. Rioux, R. M., Song, H., Hoefelmeyer, J. D., Yang, P., & Somorjai, G. A. (2004). *Journal of Physical Chemistry B*, *109*, 2192.
64. Henry, C. R. (1998). *Surface Science Reports*, *31*, 231.
65. Masson, A., Bellamy, B., Romdhane, Y., Che, M., Roulet, H., & Dufour, G. (1986). *Surface Science*, *173*, 479.
66. Ko, M. K., & Frei, H. (1805). *Journal of Physical Chemistry B*, *2004*, 108.
67. Rekoske, J. E., Cortright, R. D., Goddard, S. A., Sharma, S. B., & Dumesic, J. A. (1880). *Journal of Physical Chemistry*, *1992*, 96.
68. Mohsin, S. B., Trenary, M., & Robota, H. J. (1988). *Journal of Physical Chemistry*, *92*, 5229.
69. Zhu, J., & Zäch, M. (2009). *Current Opinion in Colloid & Interface Science*, *14*, 260.
70. Maeda, K., & Domen, K. (2007). *Journal of Physical Chemistry C*, *111*, 7851.
71. Kittel, C. (2006). *Einführung in die Festkörperphysik* Munich: Oldenbourg Verlag.
72. Wang, Y., & Herron, N. (1990). *Physical Review B*, *42*, 7253.
73. El-Sayed, M. (2004). *Accounts of Chemical Research*, *37*, 326.
74. Bao, N., Shen, L., Takata, T., & Domen, K. (2008). *Chemistry of Materials*, *20*, 110.
75. Vaneski, A. (2009). Master's thesis, Ludwigs-Maximilians Universität München.
76. Berr, M., Vaneski, A., Susha, A., Rodrigues-Fernandez, J., Döblinger, M., & Jäckel, F., et al. (2010). *Applied Physics Letters*, *97*, 093108.

77. Shemesh, Y., Macdonald, J. E., Menagen, G., & Banin, U. (2011). *Angewandte Chemie International Edition*, *50*, 1185.
78. Berr, M. J., Vaneski, A., Mauser, C., Fischbach, S., Susha, A. S., & Rogach, A. L. (2011). *Jäckel, F*. Feldmann: J. Small, *8*, 291–297.
79. Sathish, M., & Viswanath, R. (2007). *Catalysis Today*, *129*, 421.
80. Nørskov, J. K., Bligaard, T., Logadottir, A., Kitchin, J. R., Chen, J. G., & Pandelov, S., et al. (2005). *Journal of The Electrochemical Society*, *152*, J23.
81. Amirav, L., & Alivisatos, A. (1051). *Journal of Physical Chemistry Letters*, *2010*, 1.
82. Hoffmann, R. (1987). *Angewandte Chemie*, *99*, 871.
83. Cox, P. A. (1987). *The electronic structure and chemistry of solids*. New York: Oxford University Press.
84. Kittel, C. (1999). *Einführung in die Festkörperphysik* Munich: Oldenbourg Wissenschaftsverlag.
85. Ertl, G., Knözinger, H., Schüth, F., Weitkamp, J. (2008). *Handbook of heterogeneous catalysis* (2nd ed.). New York: Wiley-VCH.
86. Ertl, G., Küppers, J. (1985). *Low energy electrons and surface chemistry* (2nd ed.). New York: Wiley-VCH.
87. Norskov, J. K., Bligaard, T., Hvolbaek, B., Abild-Pedersen, F., Chorkendorff, I., & Christensen, C. H. (2008). *Chemical Society Reviews*, *37*, 2163.
88. Bligaard, T., Nørskov, J., Dahl, S., Matthiesen, J., Christensen, C., & Sehested, J. (2004). *Journal of Catalysis*, *224*, 206.
89. Falsig, H., Hvolbæk, B., Kristensen, I. S., Jiang, T., Bligaard, T., & Christensen, C. H., et al. (2008). *Angewandte Chemie International Edition*, *47*, 4835.
90. Mavrikakis, M., Hammer, B., & Nørskov, J. (1998). *Physical Review Letters*, *81*, 2819.
91. Greeley, J., Nørskov, J. K., & Mavrikakis, M. (2002). *Annual Review of Physical Chemistry*, *53*, 319.
92. Strasser, P., Koh, S., Anniyev, T., Greeley, J., More, K., & Yu, C., et al. (2010). *Nature Chemistry*, *2*, 454.
93. Kimura, K., Katsumata, S., Achiba, Y., Yamazaki, T., & Iwata, S. (1981). *Handbook of HeI photoelectron spectra of fundamental organic molecules: Ionization energies, ab initio assignments, and valence electronic structure for 200 molecules*. Tokyo: Japan Scientific Societies Press.
94. Blyholder, G. (1964). *Journal of Physical Chemistry*, *68*, 2772.
95. Kunz, S. (2010). Ph.D. thesis, Technische Universität München.
96. Crampton, A. (2011). Master's thesis, Technische Universität München.
97. Hüfner, S. (2003). *Photoelectron spectroscopy: Principles and applications* (3rd ed.). Berlin: Springer.
98. Brucker, C., & Rhodin, T. (1977). *Journal of Catalysis*, *47*, 214.
99. Demuth, J. E., & Eastman, D. E. (1974). *Physical Review Letters*, *32*, 1123.
100. Cassuto, A., Hugenschmidt, M., Parent, P., Laffon, C., & Tourillon, H. (1994). *Surface Science*, *310*, 390.
101. Kelemen, S., & Fischer, T. (1981). *Surface Science*, *102*, 45.
102. Wertheim, G. K., DiCenzo, S. B., & Buchanan, D. N. E. (1986). *Physical Review B*, *33*, 5384.
103. Cheshnovsky, O., Taylor, K., Conceicao, J., & Smalley, R. (1990). *Physical Review Letters*, *64*, 1785.
104. von Issendorff, B., & Cheshnovsky, O. (2005). *Annual Review of Physical Chemistry*, *56*, 549.
105. Wertheim, G. K., & DiCenzo, S. B. (1988). *Physical Review B*, *37*, 844.
106. Mason, M. G., & Baetzold, R. C. (1976). *Chemical Physics*, *64*, 271.
107. Mason, M. G., Gerenser, L. J., & Lee, S. T. (1977). *Physical Review Letters*, *39*, 288.
108. Takasu, Y., Unwin, R., Tesche, B., Bradshaw, A., & Grunze, M. (1978). *Surface Science*, *77*, 219.
109. Mason, M. G. (1983). *Physical Review B*, *27*, 748.

110. Eberhardt, W., Fayet, P., Cox, D. M., Fu, Z., Kaldor, A., & Sherwood, R., et al. (1990). *Physical Review Letters*, *64*, 780.
111. Fayet, P., Patthey, F., Roy, H. V., Detzel, T., & Schneider, W. D. (1992). *Surface Science*, *269–270*, 1101.
112. Roy, H.-V., Fayet, P., Patthey, F., Schneider, W.-D., Delley, B., & Massobrio, C. (1994). *Physical Review B*, *49*, 5611.
113. Wortmann, B., Mende, K., Duffe, S., Grönhagen, N., & von Issendorff, B., Hövel, H. (2010). *Physica Status Solidi (b)*, *247*, 1116.
114. Krischok, S., Höfft, O., & Kempter, V. (2002). *Nuclear Instruments and Methods in Physics Research B*, *193*, 466.
115. Stracke, P., Krischok, S., & Kempter, V. (2001). *Surface Science*, *473*, 86.
116. Krischok, S., Stracke, P., & Kempter, V. (2006). *Appllied Physics A*, *82*, 167.
117. Krischok, S., Stracke, P., Höfft, O., Kempter, V., Zhukovskii, Y., & Kotomin, E. (2006). *Surface Science*, *600*, 3815.
118. Brundle, C., & Baker, A. (1977). In C. Brundle & A. Baker (Eds.), *Electron spectroscopy: Theory, techniques and applications* (Vol. 1). New York: Academic Press Inc.
119. Niemantsverdriet, J. W. (2007). *Spectroscopy in catalysis: An introduction* (3rd ed.). New York: Wiley-VCH.
120. Brundle, C., & Baker, A. (1979). *Electron spectroscopy: Theory, techniques and applications* (Vol. 3). New York: Academic Press Inc
121. Henzler, M., Göpel, W. (2007). Oberflächenphysik des Festkörpers, unveränd. nachdr. ed. Teubner Verlag.
122. Broughton, J. Q., & Perry, D. L. (1978). *Surface Science*, *74*, 307.
123. Gadzuk, J. W. (1975). *Journal of Vacuum Science & Technology*, *12*, 289.
124. Anderson, S., & Nyberg, G. (1990). *Journal of Electron Spectroscopy and Related Phenomena*, *52*, 293.
125. Joyce, J., del Giudice, M., & Weaver, J. (1989). *Journal of Electron Spectroscopy and Related Phenomena*, *49*, 31.
126. Schweinberger, F. F., Crampton, A., Zimmermann, T., Kwon, G., Ridge, C., & Günther, S., et al. (2013). *Surface Science*, *609*, 18.
127. Harada, Y., Masuda, S., & Ozaki, H. (1897). *Chemical Reviews*, *1997*, 97.
128. Hagstrum, H. D. (1976). *Surface Science*, *54*, 197.
129. Somorjai, G., & Park, J. (2007). *Physics Today*, *48*, 293–302.
130. Stoltze, P., & Nørskov, J. K. (1985). *Physics Review Letters*, *55*, 2502.
131. Schloegl, R., Schoonmaker, R. C., Muhler, M., & Ertl, G. (1988). *Catalysis Letters*, *1*, 237.
132. Freund, H., Kuhlenbeck, H., Libuda, J., Rupprechter, G., Bäumer, M., & Hamann, H. (2001). *Topics in Catalysis*, *15*, 201.
133. Ciszewski, A., Kucharczyk, R., & Wandelt, K. (2013). *Surface Science*, *607*, 1.
134. Imbihl, R., Behm, R., & Schlögl, R. (2007). *PCCP*, *9*, 3459.
135. Somorjai, G. A., & Materer, N. (1994). *Topics in Catalysis*, *1*, 215.
136. Somorjai, G., & Park, J. (2007). *Catalysis Letters*, *115*, 87.
137. Pantförder, J. (2005). Ph.D. thesis, Friedrich-Alexander-Universität Erlangen-Nürnberg.
138. Libuda, J., Meusel, I., Hoffmann, J., Hartmann, J., Piccolo, L., Henry, C. R., et al. (2001). *Chemical Physics*, *114*, 4669.
139. Freund, H. (2002). *Surface Science*, *500*, 271.
140. Freund, H. J. (2007). *Surface Science*, *601*, 1438.
141. Goodman, D. W. (1995). *Chemical Reviews*, *95*, 523.
142. Heiz, U., Landman, U., & Henry, C. R. (2008). In U. Heiz, U. Landman (Eds.), Nanocatalysis. Berlin: Springer.
143. Heiz, U., & Bullock, E. (2004). *Journal of Materials Chemistry*, *14*, 564–577.
144. Johannson, S., Fridell, E., & Kasemo, B. (2000). *Journal of Vacuum Science & Technology A*, *18*, 1514.
145. Jacobs, P., Wind, S., Ribeiro, F., & Somorjai, G. (1997). *Surface Science*, *372*, 249.

146. Wegner, K., Piseri, P., Tafreshi, H. V., & Milani, P. (2006). *Journal of Physics D: Applied Physics*, *39*, R439.
147. Rößler, M. W. (2003). Ph.D. thesis, Freie Universität Berlin.
148. Reichelt, R. (2010). Ph.D. thesis, Ludwigs-Maximilians Universität München.
149. Hansen, T. (2006). Ph.D. thesis, Danmarks Tekniske Universitet.
150. Hansen, T. W., Wagner, J. B., Hansen, P. L., Dahl, S., Topsøe, H., & Jacobsen, C. J. H. (2001). *Science*, *294*, 1508.
151. Campbell, C. T. (2001). *Science*, *294*, 1471.
152. Rupprechter, G. (2004). *Annual Rreports Section "C"* (*Physical Chemistry*) *100*, 237.
153. Suchorski, Y., Beben, J., Imbihl, R., James, E. W., Liu, D.-J., & Evans, J. W. (2001). *Physical Review B*, *63*, 165417.
154. Henriksen, T. R., Olsen, J. L., Vesborg, P., Chorkendorff, I., & Hansen, O. (2009). *Review of Scientific Instruments*, *80*, 124101.
155. Ajmera, S., Delattre, C., Schmidt, M., & Jensen, K. (2002). *Sensors and Actuators B*, *82*, 297.
156. Fiordaliso, E., Murphy, S., Nielsen, R., Dahl, S., & Chorkendorff, I. (2012). *Surface Science*, *606*, 263.
157. Johansson, M., Lytken, O., & Chorkendorff, I. (1863). *Surface Science*, *2008*, 602.
158. Leppelt, R., Schumacher, B., Häring, T., Kinne, M., & Behm, R. J. (2005). *Review of Scientific Instruments*, *76*, 024102.
159. Langhammer, C., & Larsson, E. M. (2012). *ACS Catalysis*, *2*, 2036.
160. Tanabe, T., Nagai, Y., Dohmae, K., Sobukawa, H., & Shinjoh, H. (2008). *Journal of Catalysis*, *257*, 117.
161. Moulijn, J., van Diepen, A., & Kapteijn, F. (2001). *Applied Catalysis A: General*, *212*, 3.
162. Bartholomew, C. H. (2001). *Applied Catalysis A: General*, *212*, 17.
163. Bartholomew, C. H., & Farrauto, R. J. (2005). *Fundamentals of industrial catalytic processes* (2nd Ed.). New York: Wiley.
164. Bartholomew, C. H. (1993). *Applied Catalysis A: General*, *107*, 1.
165. Schlögl, K. (2011). Ph.D. thesis, Technische Universität München.
166. Datye, A. K., Xu, Q., Kharas, K. C., & McCarty, J. M. (2006). *Catalysis Today*, *111*, 59.
167. Hansen, T., Wagner, J., Hansen, P., Dahl, S., Topsoe, H., & Jacobsen, C. (2001). *Science*, *294*, 1508.
168. Harris, P., Boyes, E., & Cairns, J. (1983). *Journal of Catalysis*, *82*, 127.
169. Wang, B., Yoon, B., König, M., Fukamori, Y., Esch, F., & Heiz, U., et al. (2012). *Nano Letters*, *12*, 5907.
170. Campbell, C. T., Parker, S. C., & Starr, D. E. (2002). *Science*, *298*, 811.

http://www.springer.com/978-3-319-01498-2

Catalysis with Supported Size-selected Pt Clusters
Fundamental UHV and Applied Ambient Experiments
Schweinberger, F.
2014, XXI, 222 p. 136 illus., 91 illus. in color., Hardcover
ISBN: 978-3-319-01498-2